A Fast Modeling Approach for Numerical Analysis of Unreinforced and FRCM Reinforced Masonry Walls under Out-Of-Plane Loading

Jacopo Scacco[1, a], Bahman Ghiassi[2, b], Gabriele Milani[1, c], Paulo B. Lourenço[3, d]

(1) Politecnico di Milano, Department of Architecture Built Environment and Construction Engineering ABC, Piazza Leonardo da Vinci 32, 20133 Milan, Italy

(2) Centre for Structural Engineering and Informatics, Faculty of Engineering, University of Nottingham, University Park, Nottingham

(3) Department of Civil Engineering, ISISE, University of Minho, Azurém, 4800-058 Guimarães, Portugal

(a) jacopo.scacco@polimi.it

(b) bahman.ghiassi@nottingham.ac.uk

(c) gabriele.milani@polimi.it

(d) pbl@civil.uminho.pt

Keywords: FRCM Fiber Reinforced Cementitious Matrix; TRM Textile Reinforced Matrix; Masonry; Advanced numerical modeling; Homogenization approach; Heterogeneous modeling

Abstract. A new discretized homogenization approach is proposed in this study in order to predict the behavior of unreinforced and FRCM reinforced masonry structures. The proposed approach allows overcoming the common disadvantages of the existing homogenization approaches: (a) being difficult to implement and (b) not allowing to couple the in-plane and out-of-plane actions. Reference experimental results and detailed numerical modeling are used for validation of the proposed modeling strategy. In the proposed model, the elastic cells are linked by homogenized interfaces. The mechanical properties coming from the homogenization procedures are lumped at the interfaces by means of the generic Concrete Damage Plasticity model, allowing easy implementation and avoiding

computational issues peculiar to other approaches available in the literature. The new approach shows accurate results in predicting the global behavior and the damage pattern for both unreinforced and FRCM strengthened masonry walls. The results are promising also with a view to be applied for more complex reinforced applications as double curvature masonry structures.

1. INTRODUCTION

The heterogeneous character of masonry structures, along with their weak behavior under tension, make their analysis a challenging task. The need for introducing a reinforcing system, in order to reduce the vulnerability of masonry structures to seismic actions, adds a further complication in the numerical modeling procedures. A wide overview of the most diffused strengthening techniques used for improving the seismic performance of unreinforced masonry buildings is discussed in [1], which provides as well an insight into the numerical approaches used in literature. In the last five years, the application of fiber composite materials has met successively the requirements defined by guidelines, such as the ones from the International Council on Monuments and Sites. At first, after a successful application of FRP (Fiber Reinforced Polymer) on concrete substrates, the technology started to be applied also on masonry ensuring a marked increase in terms of strength and deformation, along with a relative easy execution [2]–[9]. Its effectiveness has been proved also at building-scale level, an evidence supported by non-linear numerical analyses on case studies [10].

In the case of interventions with FRP, the use of epoxy resins as matrix is able to provide an efficient bond with the masonry substrate. On the other hand, there are some disadvantages in terms of compatibility, as reported in [11]. The main issues are related to damp incompatibility, as the application of epoxies can be unsuccessful on humid surfaces. Also, the system masonry substrate – epoxy matrix may be subjected to strain incompatibilities due to different thermal coefficients. Moreover, when applying this kind of reinforcement, the vapor permeability is strongly reduced. The issues are not only related to incompatibility with the substrate, but also to the potential of harm for workers when the epoxies are applied, to its high cost and the lack of fire resistance. Last but not the least, for structures with a cultural value, it should be considered that the application of FRP is affecting the original material and, to some extent, irreversible.

Consequently, the replacement of the inorganic matrix with an organic one seems to be more suitable, still ensuring good performance in terms of mechanical capacity [12] but with a higher compatibility and less invasiveness.

The reinforcement by FRCM implies the application of at least two layers of cement-based or hydraulic lime mortar, among which fibers (Carbon, PBO, Aramid, Basalt, Glass) are embedded. Several recent experimental studies can be found in the literature on tensile and bond properties of FCRM reinforcement [13]–[19], or on their effectiveness in improving the performance of in-plane loaded walls [20]–[22] arches [23]–[26], vaults [27], [28] and pillars [29], [30]. Due to such clear benefits, such technology has been increasingly adopted for the seismic retrofitting of masonry buildings, as reported in [31]–[33], where also non-linear analyses were carried out to show the effectiveness of the intervention.

On the other hand, the behavior of walls or masonry infills under out-of-plane loads are not well investigated. In the lack of sufficient experimental results, reliable numerical models can be used for better understanding the performance of FRCM-strengthened walls under out-of-plane loads. A general review of the existing approaches for the computational analysis of masonry structures is discussed in [34]. From a numerical point of view, modeling such masonry elements could be highly demanding, as it could be necessary to take into account different materials interacting with distinct material properties. In this context, the use of a detailed 3D micro-modeling approach may be unavoidable [35]-[36], at the same time requiring prohibitive computational costs. The use of a macro-modeling technique, where bricks and mortar are replaced by a homogenous orthotropic material with fictitious properties, requires much less computational burden but also an extensive preliminary campaign in order to calibrate the model [37]. Homogenization procedures [38]–[40] can address both challenges and proved to be highly effective when applied to a composite material as masonry. In these approaches, the average properties are defined by means of a Boundary Value Problem written on a unit cell (RVE) considered as representative of the wall, without the need to perform costly experimental campaigns. The homogenized material is orthotropic with a softening post-elastic behavior both in tension and in compression and exhibits the same numerical advantages of a macro-modelling procedure. In this way, the properties coming from homogenization can be transferred to the structural level in terms of an averaged isotropic material. Otherwise, the orthotropic behavior can be preserved by using a discrete approach where the

non-linearities are lumped only at the interfaces joining elastic or rigid elements. The rigid body-spring approach "RBSM", applied in [41]–[43], is also interesting and consists of modeling the structure as a repetition of rigid cells connected by nonlinear springs. However, the definition of interfaces by springs and rigid offsets is not straightforward, because still presents the necessity to keep uncoupled the in and out of plane loads.

In this paper, a novel homogenization approach is adopted. The brick/blocks are considered as purely elastic and linked by interfaces where all the non-linearities are lumped [44]. The model takes advantage of an already implemented constitutive softening model available in the FEM software Abaqus called CDP Concrete Damage Plasticity model. CDP, originally developed for modeling concrete, is suitable for brittle and quasi-brittle materials, resulting adaptable for masonry. Afterward, FCRM is modeled directly on the homogenized model by means of elasto-plastic trusses, simulating the fiber net embedded in the cementitious matrix, again modeled with CDP. With reference to some experimentation carried out in [45], the unreinforced case has been also studied in order to calibrate the model and to discuss the obtainable match with experimental results without FRCM, providing as well an insight into the seismic upgrade that can be obtained by such reinforcement. In the Appendix, it is then provided a further improvement of the proposed approach, introducing cohesive surfaces to properly simulate local out-of-plane sliding of the wall.

The advantages of the proposed model are highlighted by a comparison with experimental data [45], along with the results coming from a detailed 3D micro-modeling. A good match between the two different numerical approaches and experiments is obtained, both in terms of load-displacement curves and in the evolution of damage patterns.

2. REFERENCE EXPERIMENTAL DATA

The experimental tests taken as reference were carried out by the Department of Structures for Engineering and Architecture at University of Naples "Federico II". The program included testing unreinforced and FCRM reinforced walls under out-of-plane loading [45]. The dimensions of each clay brick were equal to 250×55×120 (mm^3), with an overall dimension of the wall equal to 1515×1755×120 (mm^3). The average thickness of the mortar joints was around 10.5 mm. The main goal of the experiment was to reproduce the condition of a typical infill wall in the context of an RC building. In order to pursue this task, special care was taken to reproduce

consistent boundary conditions. The top edge was considered unconstrained as the usual low level of connection with the beam above. As well, one lateral edge was left free, simulating the presence of an opening. The basis of the wall was considered simply supported, being the wall just located on a layer of mortar inside a steel profile UPN 280. The opposite lateral edge was supported as a clamp, simulating a connection with an orthogonal wall, by means of a steel profile UPN180 connected in three points to a rigid steel frame. The asymmetrical lateral boundary conditions led to a biaxial response of the wall, making possible the evaluation of the strengthening for a bidirectional stress state. FRCM application consisted of two layers of inorganic matrix on one side of the wall, along with a mesh 6x6 (mm) of basalt fibers. The perpendicular load, with the aim to induce a more demanding stress state, was applied by displacement control at the top corner, through a steel plate, applied on the reinforced side (**Figure 1**).

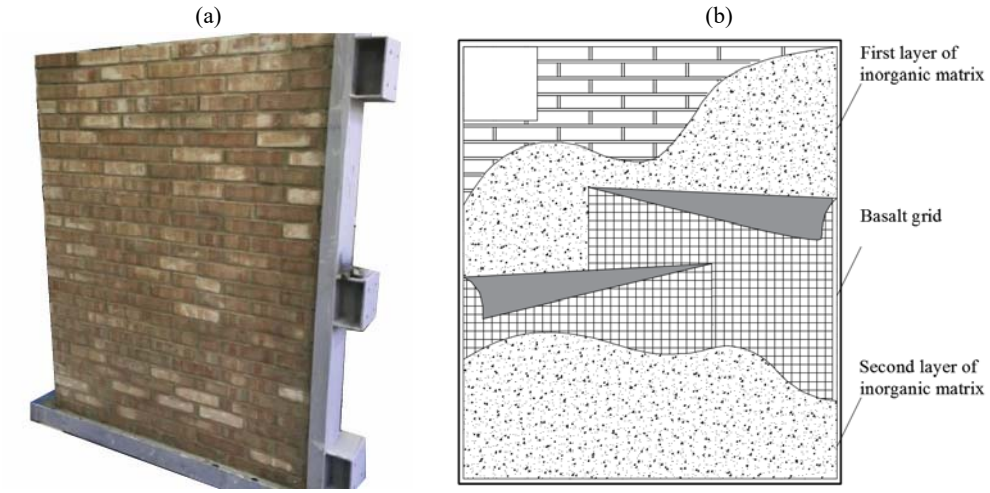

Figure 1. Experimental set-up of the tested wall: (a) unreinforced panel [45]; (b) reinforced configuration.

The results are re-proposed in this section as reference for the following numerical analyses. In terms of crack pattern, the unreinforced wall showed a stepped crack pattern developed from the top corner of the constrained edge. The damage is led by the arrangement of the bricks and by their high mechanical properties, involving only the mortar and the interfaces. The load-displacement curve, measured at the point of the application of the load, is characterized by an elastic response until 1.5 kN, followed by a gradual loss of stiffness until 3.0 kN. Afterwards, collapse occurred with a marked softening branch, reaching an ultimate displacement of 10 mm. The damage of the reinforced wall is reported only for the unreinforced side, where

the cracks are concentrated nearby the steel plate. In terms of Load-Displacement, the curve could be idealized as a tri-linear one. A first elastic branch until 3.8 kN, followed by a second branch with a reduced stiffness until a value of 6.0 kN. Once this value is reached, a plateau is recorded until a displacement of 60 mm (**Figure 2)**.

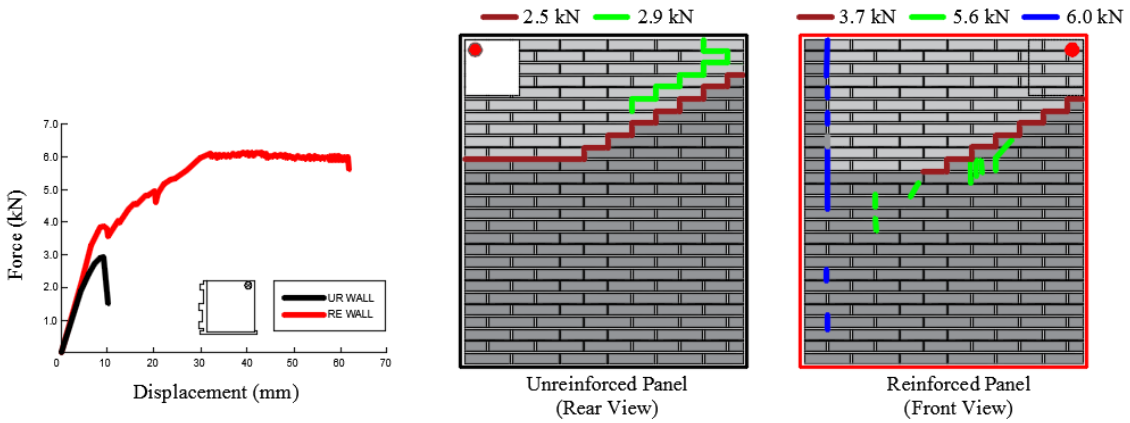

Figure 2. Experimental load-displacement curve and damage pattern of the unreinforced and reinforced walls.

3. FINITE ELEMENT MODELING

The experimental tests are numerically reproduced by means of two different approaches. The first one involves a detailed micro-modeling of both unreinforced and reinforced wall to provide a useful reference for the new discretized homogenization model, the second approach, proposed in this work.

Both approaches are carried out in the ABAQUS FEM package. The nonlinear properties of materials are considered through the already implemented constitutive model Concrete Damage Plasticity. CDP model was originally developed for exploring the non-linearities peculiar to concrete. However, as suggested by many researchers, the model is applicable to brittle and quasi-brittle materials such as bricks and mortar. CDP is characterized by a multi-dimensional elasto-plastic yield surface, and its evolution depends on the uniaxial damage failure model under tension and compression. The failure surface corresponds to the Drucker-Prager yield function, which eventually is switched to a Mohr-Coulomb criteria through a parameter Kc (**Figure 3**).

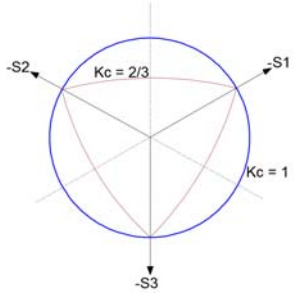

Figure 3. Drucker-Prager and Mohr-Coulomb failure surfaces implemented in Abaqus.

The surface is regularized by application of a parameter called "eccentricity" in order to avoid numerical instabilities. The distinct behavior under tension and compression is introduced following an exponential or linear softening in tension, and a parabolic softening in compression. The respective degradation of the elastic stiffness is governed by two variables d_t and d_c, which are functions of the plastic strain. The damage variables vary in the range of 0.0 (undamaged material) to 1.0 (total loss of strength). In order to define the post-peak behavior under tension, a fracture energy can be input directly as a property of the material. This approach allows a linear softening in tension [46] and it is used in this work. **(Figure 4).**

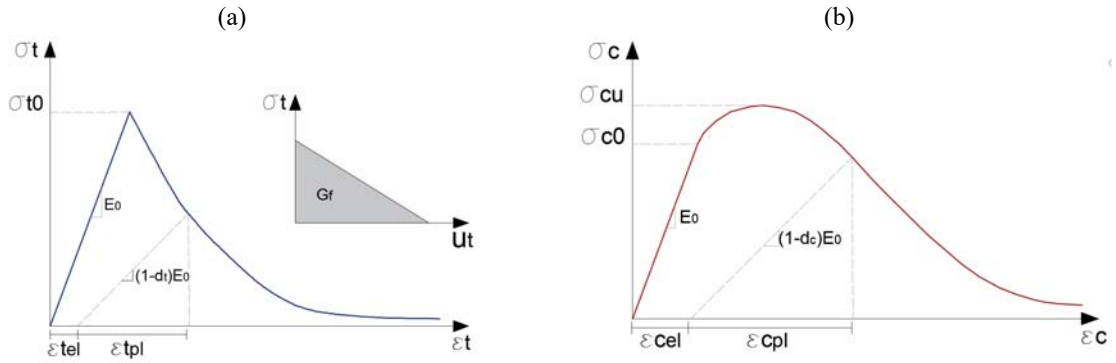

Figure 4. Constitutive behavior in tension (a) and in compression (b).

The viscosity parameter is assumed, usually, in a range of 0.0001-0.0005. After some sensitivity analyses, a value of 0.0003 resulted in a fair compromise to ensure reliable results and to tackle convergence issues. The values used in the analyses to define the yield surface are provided in **Table 1**:

Table 1. Input parameters in the Concrete Damage Plasticity.

Dilatation Angle ψ	**Flow Potential Eccentricity e**	**K_c**	**Viscosity Parameter**
10°	0.1	0.667	0.0003

3.1. Micro-modeling Approach

As mentioned, in order to have a reliable numerical reference, the first part of the work is devoted to the definition of a refined micro-modeling of both unreinforced and reinforced panels.

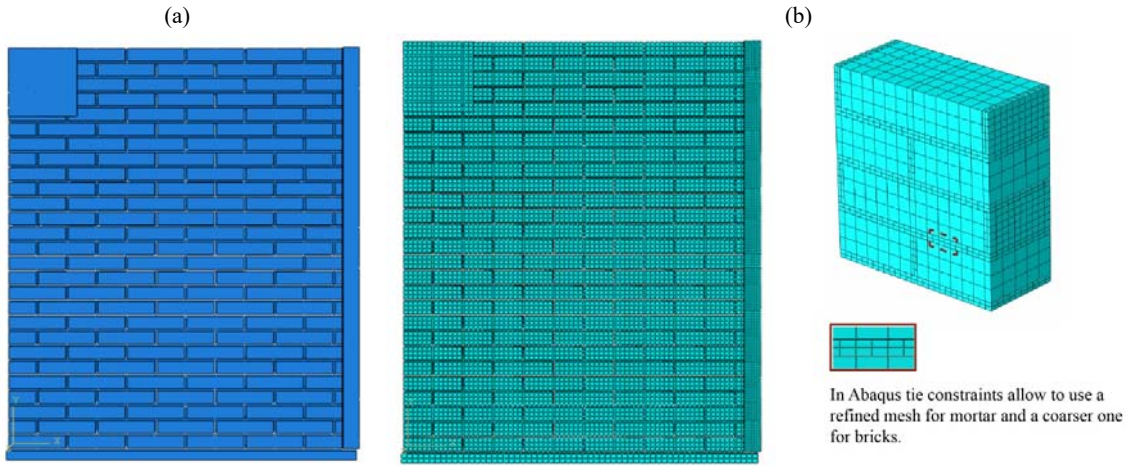

Figure 5. Geometric configuration (a) and discretization (b) of the unreinforced panel in Abaqus.

In the full heterogeneous 3D approach, bricks, mortar and the reinforcement, made of cementitious mortar and basalt fibers, are meshed separately. Linear 8-nodes brick elements are used for mortar, bricks and reinforcement matrix (see **Figure 5**), whereas mesh fibers are simulated as 2-nodes trusses embedded within the two layers of the cementitious mortar (**Figure 6).** As highlighted in [42], a rigorous approach when FRCM reinforcement is applied should involve the full modeling of the basalt grid, taking into account its fragile behavior along with the possibility of slipping of the fibers inside the mortar. The difficulties from the computational point of view are evident which make simplification of the model necessary. Again in agreement with [42], the mesh of the grid, in reality with a narrow spacing equal to 6 mm, is modeled with a step of about 35 mm, taking care to locate the trusses along the nodes belonging to the bricks elements of the mortar. In order to consider the same amount of reinforcement, the cross-sections of the fibers are increased accordingly to the step introduced in the numerical model.

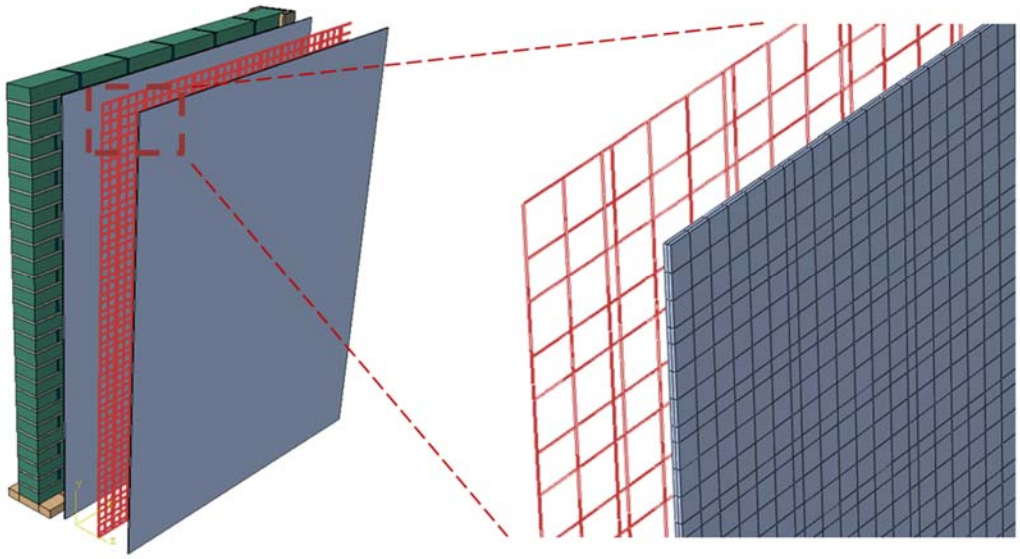

Figure 6. Geometric configuration and discretization of the strengthening.

An elasto-plastic behavior of the fibers is accounted in order to tackle some computational issues (**Figure 7**), along with a perfect bonding with the layers of the mortar.

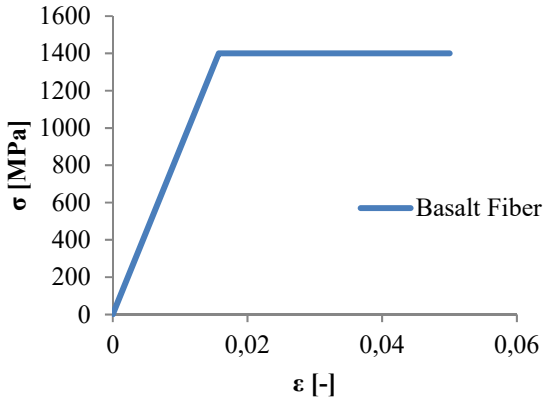

Figure 7. Stress-strain curve for the tensile behavior of basalt fibers.

As well, the debonding between the masonry substrate and the cementitious mortar is not introduced in the present model, because less likely to occur in FRCM cases [47]. The matrix is realistically modeled as two separate layers, each discretized with two linear solid elements along the thickness (**Figure 6**). The mortar joints are more refined than the bricks, ensuring at least two elements in the thickness, in order to model properly where the damage is more likely to occur (**Figure 5**). Along the depth the joints present 10 elements, whereas

bricks exactly the half, reaching an overall number of 140115 elements for the unreinforced case and few more elements for the FRCM reinforced one. Concerning the boundary conditions, particular care is addressed to reproduce the lateral constraint designed during the experimental stage. So, the beam UPN180 is modeled, along with the infill mortar used to cover the gap with the wall, and fixed in three different areas where the steel frame was connected. Following the experimental plan (see details in **Figure 1**), the opposite edge and the top one are considered as free, whereas the bottom is simply supported.

The material properties are synthesized in **Table 2.** The bricks have an elastic modulus equal to 4.0 GPa, the joints to 1.4 GPa, the cementitious mortar to 8.0 GPa, and the fibers equal to 89 GPa.

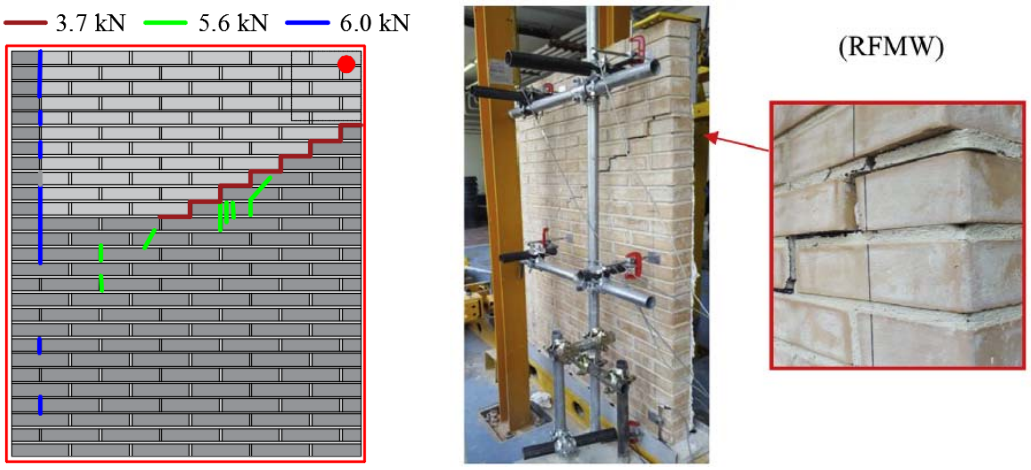

Figure 8. Experimental damage pattern of the reinforced panel.

For the mortar joints, it is assumed a compressive strength f_c equal to 12 MPa, and for cementitious matrix a mortar with f_c equal to 15 MPa (in agreement with experimentations carried out in [45]). The values of compressive strength are taken from the reference experimental results, while the tensile strengths are chosen as 10% of compressive strength for the matrix of the strengthening system, and 0.25 MPa for the mortar joints, which is in agreement with a mortar type M2.5 as Eurocode 6 classification. These latter values are justified considering that in [45] the mechanical characterization of the brick-mortar interfaces is missing. Indeed in [45], the mortar mechanical properties experimentally determined appear extremely high and they would be related to a very high collapse load in the numerical simulations. On the other hand, the observed failure (see

Figure 8) shows clearly an out-of-plane sliding of the brick-mortar interfaces, which are not experimentally characterized in [45]. As a consequence, the authors assumed for mortar weaker mechanical properties to properly take into account that failure occurs at the brick-mortar interface and not in the mortar bulk, which results in practice undamaged at the ultimate limit state. Moreover, as no information about the kind of failure experienced by the strengthening is available from the test, a reasonable reduction of the characteristic tensile strength (1542 MPa) of the fibers is applied by means of a factor equal to 1.1.

The inelastic behavior in tension, in the post-peak range, is characterized by the introduction of a reliable fracture energy, an input available in Abaqus that allows tackling mesh sensitivity issue, peculiar to a stress-strain input. In **Figure 9,** tensile stress-crack width relationship assumed for mortar joints is plotted. In **Table 3**, damage coefficients d_t assumed in the analyses at different stresses and crack widths are summarized, imposing a linear variation of the damage parameter. In the following section, a sensitivity analysis of different values of fracture energy applied to the unreinforced model is provided. The inelastic behavior in compression is defined in Abaqus with a stress-strain criterion approximating a parabolic softening. The corresponding curves and coefficients of damage d_c are presented in **Figure 10** and **Table 4** respectively.

Table 2. Mechanical properties of the materials for the numerical simulations.

	Young's Modulus [MPa]	**Compressive strength [MPa]**	**Tensile strength [MPa]**	**Fracture energy [N/mm]**
Bricks	4000	30.0	6.00	0.100
Mortar Joints	1400	12.0	0.25	0.025
Cementitious Matrix	8000	15.0	1.50	0.050
Basalt Fiber	8900	/	1542/1.1	/

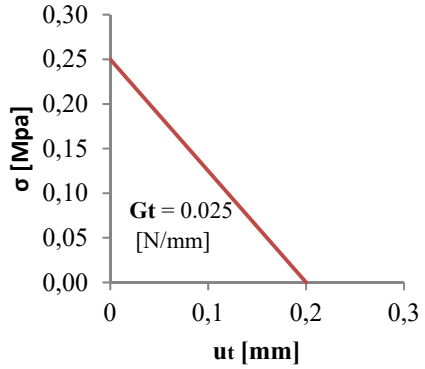

Figure 9. Non-linear mechanical properties in tension assumed for mortar joints

Table 3. Damage parameters d_t in tension (dt varies linearly between the two extreme values indicated in the table).

	σ_t [MPa]	u_t [mm]	d_t [-]
Mortar Joints	0.25 0	0 0.20	0 0.9
Cementitious Matrix	1.50 0	0 0.067	0 0.9
Bricks	6.00 0	0 0.033	0 0.9

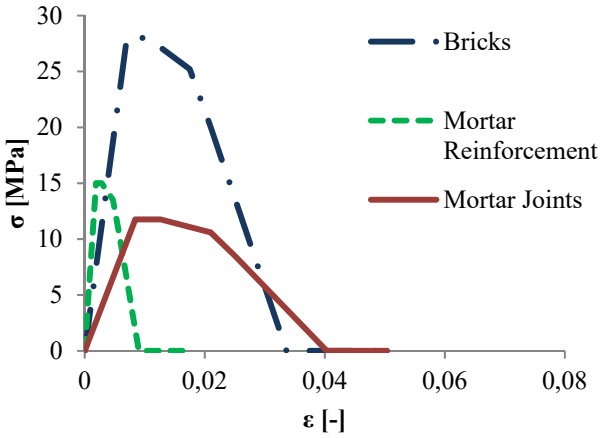

Figure 10. Non-linear mechanical properties in compression.

Table 4. Damage parameters in compression.

	σ_c [MPa]	ε [-]	d_c [-]
Mortar Joints	12.0 0.01	0.008 0.04	0 0.9
Cementitious Matrix	15.0 0.01	0.00018 0.009	0 0.9
Bricks	30.0 0.03	0.007 0.03	0 0.9

3.2. Two Step Discrete Homogenization Model

In this section, a 2-step discrete homogenization model is proposed. Instead of applying the homogenized masonry properties to a continuum, here the model is described by a repetition of elastic units linked by solid elements, where the non-linearities are lumped by means of the already discussed CDP. Different mechanical properties are addressed to the vertical and horizontal joints (or diagonal, as it will be proposed). In this way, a

differential behavior is induced along two directions to properly model the orthotropic behavior of masonry. The homogenized parameters (**Table 5)** are obtained by the application of consolidate procedures deeply discussed in [44].

Table 5. Mechanical properties coming from the homogenization.

	Homogenized Parameters	**[MPa]**
Vertical Stretching	Young Modulus E_{yy}	3125
	Tensile Strength f_{yt}	0.25
Horizontal Stretching	Young Modulus E_{xx}	4000
	Tensile Strength f_{xt}	1.00

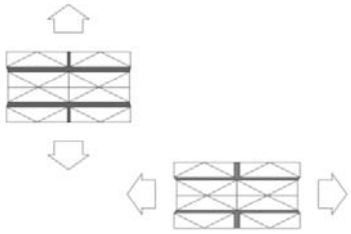

The main advantage of the method is the innovative implementation of the homogenized parameters at the structural level. A comparison could be done with the approach used in [42], [43] where rigid cells are linked by non-linear springs and rigid offset. The nature of this latter implementation involves the necessity to keep the in- and out-of-plane effects uncoupled, and to address all the elastic deformability on the joints. In the approach proposed here, on the contrary, it is possible to apply the elastic properties, coming from homogenization, directly to the units, modeled as elastic, ensuring better stability when the non-linear behavior is explored.

The use of this homogenization procedure is justified by the need to discretize with a much less refined mesh, in comparison with micro-modeling, ensuring at the same time good results, as shown in the next sections. With the aim to reproduce a damage pattern similar to the one encountered during the experimental tests, some analyses have been conducted in order to define the most suitable mesh to use in the homogenized case. The damage pattern coming from the tests results to be strongly related to the texture of the bricks. Because of their good mechanical properties, along with the asymmetric boundary conditions, the damage is enforced to occur in zigzag inside joints. For these reasons, the stepped crack peculiar to the unreinforced wall is reproducible with much more difficulties using parallelepiped discretization. As a consequence, authors experienced that wedge shaped elements are more convenient in such kind of problems, ensuring good convergence and

maintaining the computational burden small. In such a discretization, the non-linear properties are lumped in horizontal and diagonal interfaces (**Figure 11**).

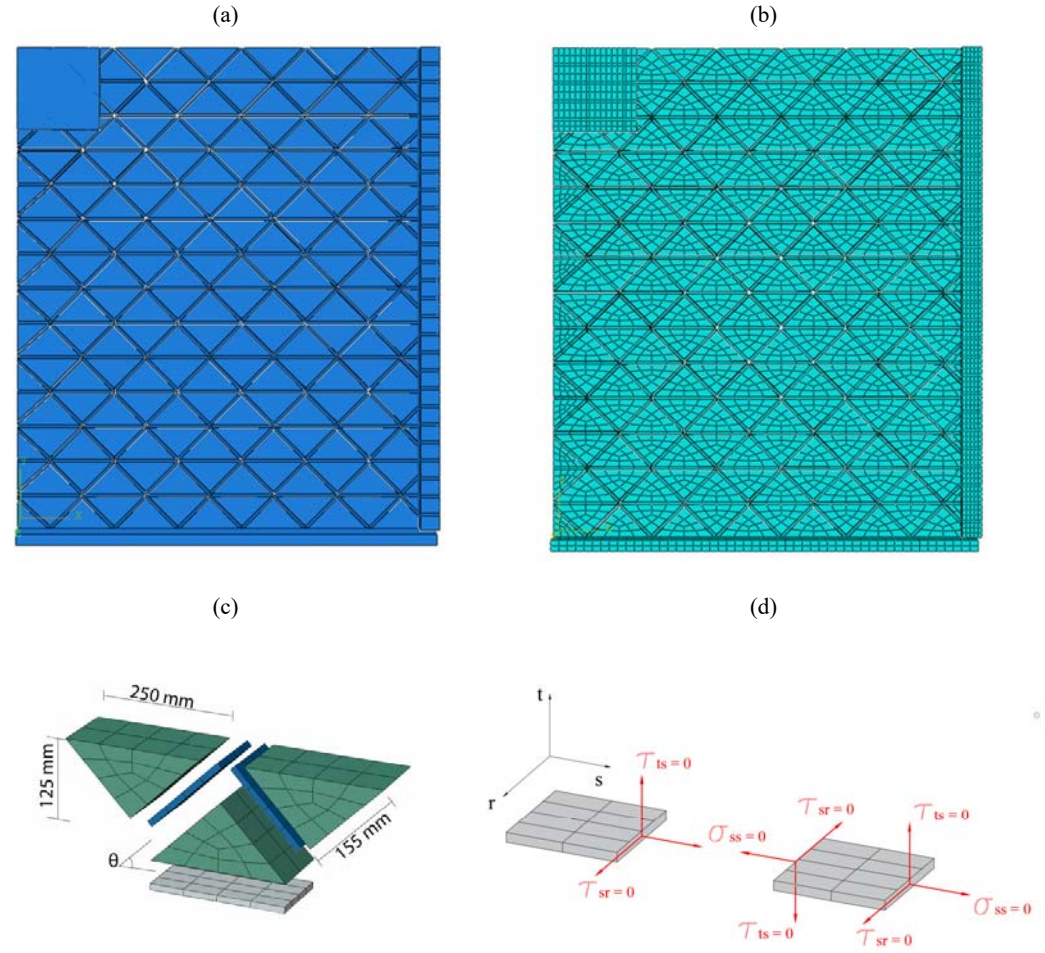

Figure 11. Geometric configuration (a) and discretization (b) of the homogenized unreinforced panel;
(c) detail of the discretization of elastic cells and interfaces;
(d) state of stress of interface in the plane *t-r* between two adjacent solid elements.

Since, the mechanical properties coming from homogenization are related to the vertical and horizontal directions, it is necessary to compute the value of the tensile strength associated to the diagonal interfaces as follows:

$$f_{t\_diagonal} = \sin\theta * f_{yt} + \cos\theta * f_{xt} = 0{,}8\ \text{MPa} \qquad (1)$$

where $\theta$is indicated in **Figure 11**.

The relative fracture energy is then homothetically scaled from the value used for micro-modeling to a value equal to 0.08 N/mm. Once the homogenized properties are obtained for the diagonal and horizontal interfaces,

the implementation in Abaqus follows the same approach used for the micro-modeling analyses, where the tensile strength is used as input along with a fracture energy criterion (**Table 6)**.

Table 6. Non-linear properties of the homogenized material in Abaqus.

	G_t [N/mm]	σ_t [MPa]	u_t [mm]	d_t [-]
Diagonal Interfaces	0.080	0.80 0	0 0.20	0 0.9
Horizontal Interfaces	0.025	0.25 0	0 0.20	0 0.9

Regarding the discretization, 4 elements are utilized along the depth and length of the interfaces with one element in the thickness. As well, the elastic units are divided by 4 elements along each edge in the plane, and by two elements in the depth, needing for the entire wall a total number of 2280 elements (**Figure 11**). The reinforced materials are then applied directly to the homogenized model in a second step, with the same procedure of the micro-modeling models. The typology and number of elements of the cementitious matrix and of the trusses are kept equal to the previous analysis, in order to have a consistent comparison between detailed heterogeneous and homogenized models.

It is important to highlight that the homogenized interfaces, made by solid elements, thanks to the typology of mesh used (with holes at the points of intersection of concurring interfaces) exhibit in practice a state of stress that approximates that of a zero-thickness interface. As a matter of fact, the authors experienced that the components of the stresses acting on the *t-r* plane (see **Figure 10d)** between two adjacent parallelepiped elements, are very close to zero and hence they can be considered negligible. In any case, a user defined element implemented in a Fortran-subroutine in Abaqus has been implemented enforcing that stresses σss, τ_{sv}, τ_{st} (see **Figure 10d)** are assumed equal to zero, so enforcing that such 3D elements behave rigorously as an interface, which however in the discretization remains with a thickness different from zero.

4. RESULTS

The results obtained from the two above approaches are presented and compared with the experimental outcomes in this section. The results are shown in terms of load-displacement curves and damage pattern, taking

advantage of the variable DAMAGET peculiar to CDP model, which describes the extent of degradation during the load history. The analyses are conducted under displacement control, which is better than load control to catch the post-peak behavior in presence of softening.

4.1. Micro-modeling Approach

With the aim of creating a sort of numerical reference for the proposed discrete homogenized approach, the results coming from micro-modeling are presented first, for both unreinforced and reinforced walls. As no information about the post-peak behavior of the mortar is available, a sensitivity analysis regarding three different values of fracture energy Gt is carried out on the unreinforced model. A good fitting of the experimental results is obtained when a Gt equal to 0.025 N/mm is assumed, reproducing in practice the same load-displacement curve obtained experimentally. The reached peak load is equal to 3 kN along with an ultimate displacement of about 10 mm (**Figure 12).**

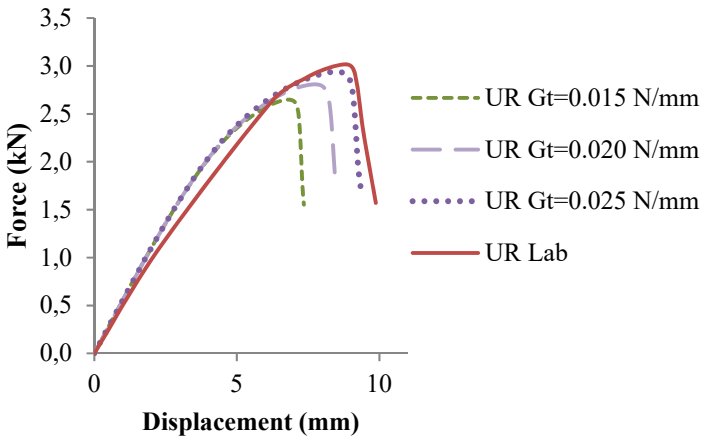

Figure 12. Comparison in terms of load-displacement curves of the results obtained experimentally and by the micro-modeling approach for different values of G_t (unreinforced panel).

Even the damage pattern is very similar to the actual failure mechanism, which in the numerical model develops following a curved yield line starting from the constrained top corner, see **Figure 13**. The only visible difference concerns the extension of the crack, that in the test is constituted by two straight yield lines, the inclined one stopping at 2/3 of the wall height and the horizontal one. This difference is however considered acceptable and does not affect the global behavior of the unreinforced wall.

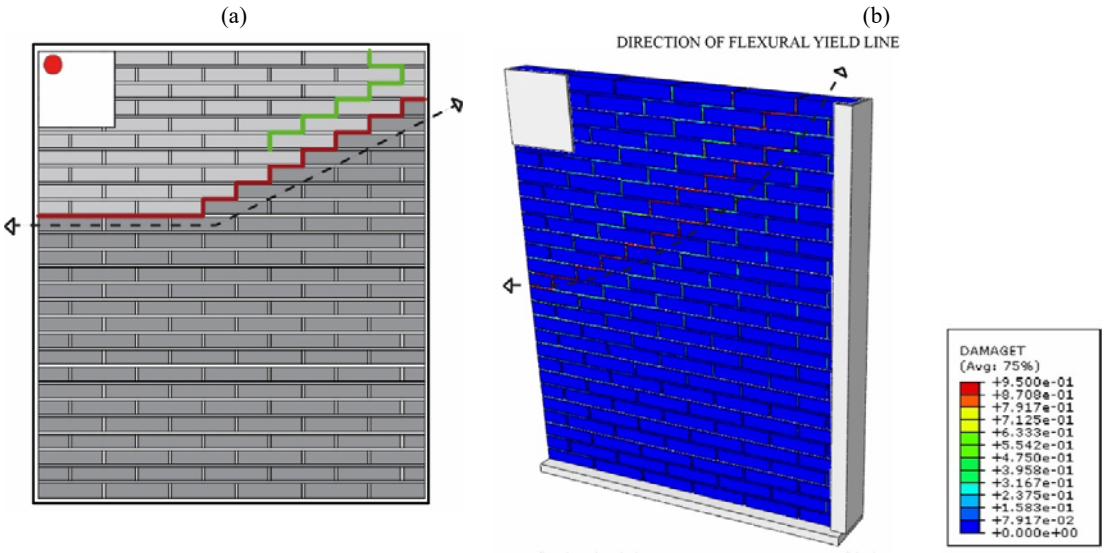

Figure 13. Experimental (a) and numerical (b) crack patterns of the unreinforced panel (micro-modeling approach).

Once the unreinforced model is calibrated, the two layers of the cementitious matrix and the basalt fiber mesh are applied in order to replicate the behavior of the reinforced panel. As can be observed in **Figure 8** and in **Figure 14** the damage pattern, only presented in [45] for the unreinforced side, is close to the experimental one. The damage, from lab tests, results to be quite severe nearby to the steel plate, then developing smoothly up to the half-length of the wall. The micro-model of the reinforced panel is able to catch such a behavior, reproducing the crack below the steel plate. It is worth noting that the failure occurred in the experiment is a kind of out-of-plane shear failure, with a consequent sliding that is very hard to reproduce numerically when interfaces among bricks and mortar are not introduced.

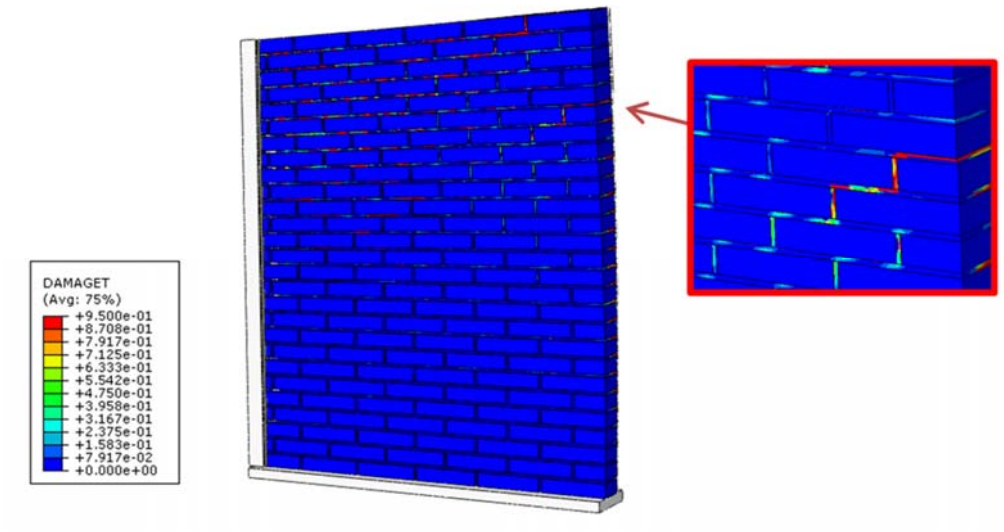

Figure 14. Numerical results of the reinforced panel (micro-modeling approach).

In terms of load-displacement curves, as can be observed in **Figure 15,** the global behavior is also well approximated considering the obtained peak load (6 kN) and maximum displacement (56 mm).

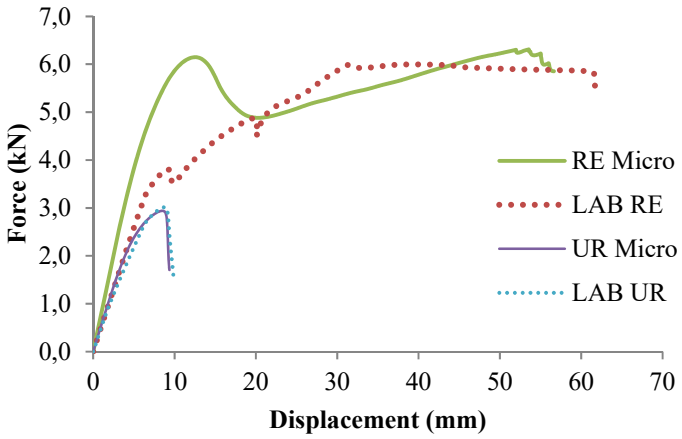

Figure 15. Comparison in terms of load-displacement curves of the results obtained experimentally and by the micro- modeling approach for the reinforced (RE) and unreinforced (UR) panels.

4.2. Two Step Discrete Homogenization Model

The homogenization model at the cell level has been already discussed in [44]; for this reason details on the model are not reported here, for the sake of conciseness. The reader interested in the implementation and validation of the model for in-and-out-plane loaded walls is referred to [43] and [48]. Once that experimental

and numerical references are provided, the results obtained with the discrete homogenized model can be finally discussed. As mentioned previously, the damage pattern is strongly dependent on the configuration of bricks and the asymmetric boundary conditions. For this reason, certain care is necessary in order to select the most convenient shape for the elastic cells of the homogenized model. In fact, the implementation of the homogenized parameters at a structural level implies that the non-linear homogenized properties are lumped exclusively at the interfaces. Consequently, the use of a parallelepiped discretization, with horizontal and vertical interfaces, would have led to a mechanism of collapse deviating from the real one (see **Figure 16**) and to an overestimation of the load carrying capacity.

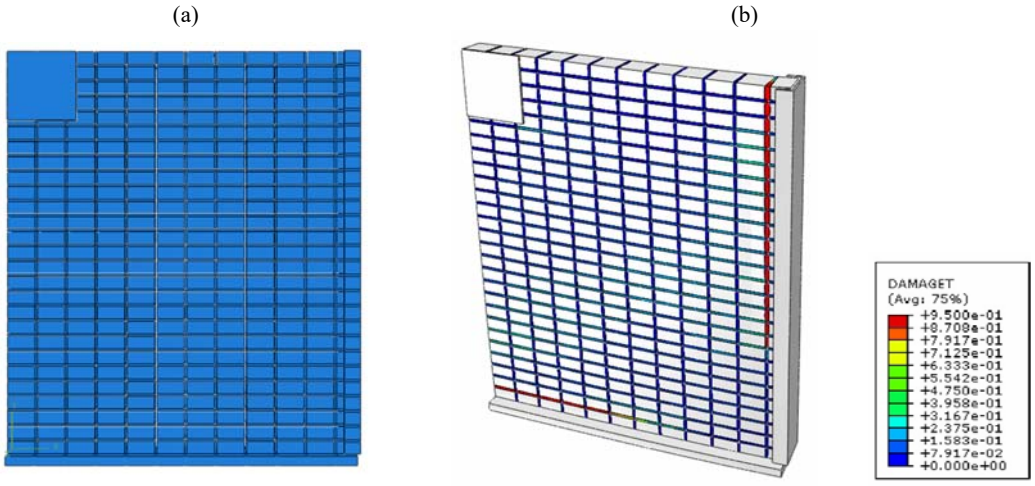

Figure 16. Geometric configuration and damage pattern of the homogenized model (parallelepiped discretization).

As a matter of fact, the damage tends to spread along the lateral constraint from the top to the bottom, progressively missing the actual evolution of damage. For this reason, wedge shaped-units are introduced in order to closely approximate the real direction of the crack (**Figure 17**).

Indeed, regarding the unreinforced panel, it is noticeable from the pictures describing the spread of the variable DAMAGET, that through this approach the damage pattern is reproduced with high accuracy. Moreover, the crack direction is closer to the real one than the one found with micro-modeling. In fact, the diagonal crack, which approximates the stepped one, extends along a horizontal direction.

(a) displacement 6 mm

(b) displacement 7 mm

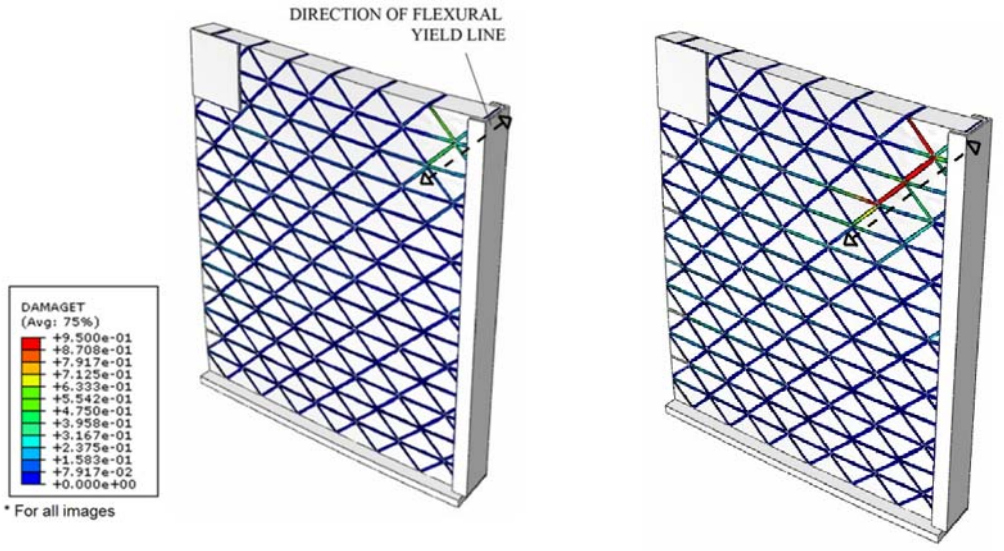

(c) displacement 8 mm

(d) experimental crack pattern

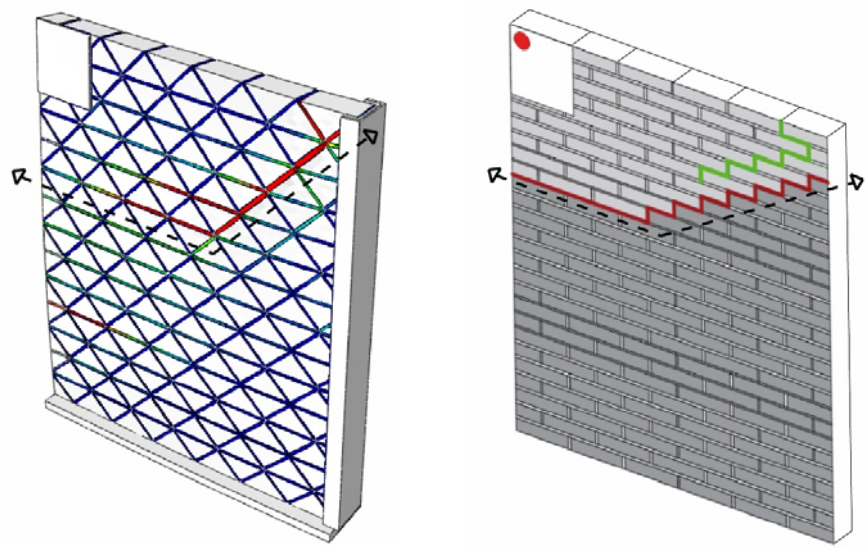

Figure 17. Evolution of the damage pattern of the unreinforced homogenized model.

Also in terms of load-displacement curves the results are found very satisfactory. The load carrying capacity is around 3 kN with the global displacement of around 10 mm. The first branch does not show a slight reduction in stiffness as in the micro-model case, so the softening behavior is reached earlier at 6 mm. The post-peak branch is less sudden and develops with a gradual loss of stiffness as indicated in **Figure 18.**

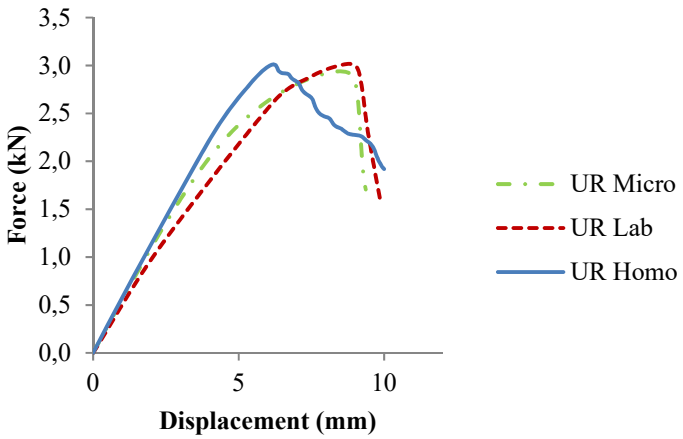

Figure 18. Comparison in terms of load-displacement curves of the results obtained experimentally, with the micro-modeling approach, and by the homogenized model (unreinforced panel).

The numerical response of the homogenized reinforced panel follows the micro-modeling result, with an elastic response until a load value of 6.2 kN. Afterwards, a slight softening branch is observed, followed by the curve approaching the plateau of the experimental curve up to a displacement of around 40 mm (**Figure 19)**. It is necessary to highlight that the final part of the third branch is likely related to a sliding phenomenon. Moreover, the ductility of the homogenized model is, in some way, limited by the less number of non-linear interfaces, as the height of one triangular unit contains two bricks of the real wall. Also, the decision of limiting the number of used elements to one along the thickness of interfaces, might limit the displacement capacity of the model. The homogenized approach, as it is conceived, is unlikely to be able to reproduce this kind of failure at large displacements, but the results in terms of global behavior and capacity load turn out to be highly satisfactory. It is worth noting how the load-displacement response of the homogenized model is characterized by a softening branch much less marked than the one observed in the micro-modeling results (**Figure 19**). This difference has to be related to the choice made during the creation of the numerical model. The fiber spacing increased to 35 mm may affect the 2-D contribution of the reinforcement when the stepped crack starts to spread, delaying the activation of the fibers. On the contrary, in the homogenized model, being the crack purely diagonal, the vertical and horizontal basalt fibers act simultaneously, leading to a result closer to the experimental ones.

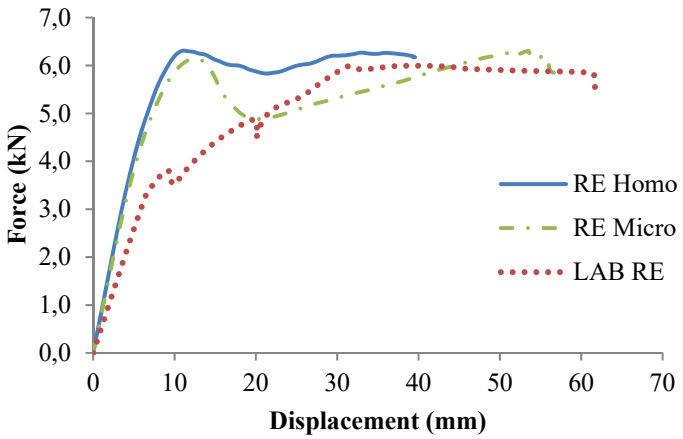

Figure 19. Comparison in terms of load-displacement curves of the results obtained experimentally, with the micro- modeling approach, and by the homogenized model (reinforced panel).

In terms of crack pattern, a slight concentration of damage is observed just behind the steel plate, where the load is applied (**Figure 20)**. The reduced number of variables and of non-linear elements does not allow to simulate accurately the evolution of damage due to a concentrated load. However, the model provides useful information about the localization of the damage, matching globally the experimental results.

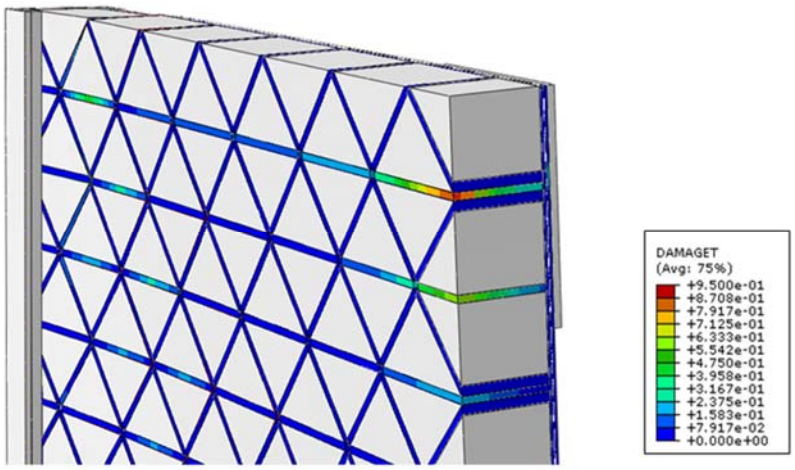

Figure 20. Damage pattern of the reinforced homogenized model in correspondence of a displacement of 40 mm.

5. CONCLUSIONS

Starting from experimental tests on unreinforced and reinforced masonry panels loaded out of plane, different numerical approaches have been presented, in order to show the advantages related to their reliability. At first, a detailed 3D micro-modeling was carried out by means of Abaqus, obtaining a numerical reference and an insight into computational requirements. Bricks and mortar have been modeled separately, addressing the non-linear properties through the Concrete Damage Plasticity, a constitutive model available in Abaqus, conceived for brittle and quasi-brittle materials. As well, in the reinforced case, the cementitious matrix and the fibers were introduced as distinct materials. The results matched in a satisfactory way with the experiments.

Afterward, a new discrete homogenization method was discussed. The main goal of the paper was indeed the proposal of an alternative approach in introducing the homogenized parameters at the structural level. The available homogenization methods used in the literature for simulating the nonlinear response of unreinforced and FRCM reinforced masonry are tricky to implement and do not allow coupling of the membrane and the out of plane actions. On the contrary, the here presented method took advantage of the same CDP used in the micro-modeling, making much easier the setup. The homogenized models are constituted by a repetition of elastic cells linked by 3D damaging bricks, where the non-linearities are lumped. The homogenized mechanical parameters were determined through consolidated approaches, deeply discussed in [36], and then applied according to the mesh pattern of the models.

In fact, the specific configuration of the wall and the failure modes experimentally observed suggested utilization of a triangular mesh suitable to reproduce properly the evolution of damage. The results showed the efficiency of the proposed homogenization approach in replicating both experimental and detailed numerical modeling, both in terms of crack spreading and load-displacement curves, reducing by far the needed computational time. It is worth mentioning that, as far the computational burden is concerned, micro-models, both in the unreinforced and reinforced cases, required a computational effort roughly ten times higher than the corresponding homogenized approaches. The authors believe that this combination of easy-implementation, accuracy, and speed, may lead to interesting future applications, even for more complex reinforced structures as vaults and domes.

6. APPENDIX COHESIVE ELEMENTS

The utilization of cohesive interfaces in combination with CDP elements where cracks are lumped helps in better identifying the failure mechanism and out-of-plane sliding. As already mentioned, the damage pattern of the reinforced panel is characterized by a sliding phenomenon just under the steel plate, where the concentrated load is applied. As the previous analyses are not fully consistent in the reproduction of this kind of behavior, here a further approach is proposed. In order to simulate properly the failure modes (tensile cracking and shear sliding) of the brick-mortar interfaces, a surface-based cohesive behavior is added to the CDP solid elements used previously for the analyses presented in the main body of the paper. These elements are already available in the Abaqus library and successfully applied to masonry structures in [49], turning out to be a reliable method for capturing crack propagation. The implementation for such surfaces is based on the definition on an initial linear elastic traction-separation law, followed by a damage initial criterion and a damage evolution law. The reader is referred to [49] for a more detailed discussion about the interaction properties and their implementation.

The traction separation model that is already available in Abaqus requires the definition of an initial elastic behavior and a criterion for the initiation and evolution of damage. In the simulations, a default contact enforcement method is used. The damage initiation selected is defined in Abaqus as “Maximum Nominal Stress”. In such approach, the damage is assumed to start when one component among the tangential and the normal one reaches its correspondent maximum value. Indeed σ_n^0, σ_s^0, σ_t^0 represent the peak values of the contact stress when the separation is either purely normal to the interface or purely in the first or the second shear direction, see [46]. In order to be consistent with the analyses discussed in the body of the paper, a value of 0.25 MPa is chosen for such strength values.

Regarding the damage evolution law, a fracture energy approach is selected. The fracture energy is defined as a property of the cohesive interaction with a linear softening behavior. Several fracture criteria are available in the Abaqus library. For the following simulations, a Benzeggagh-Kenane BK criterion is used as it results useful when the critical fracture energies during separation purely along the first and the second shear directions

are the same [46]. Even in this case, the value of the fracture energy is assumed equal to 0.025 N/mm in order to be consistent with the previous analyses. The exponent of the BK law is set equal to 2 as suggested in [49].

As the main goal of this section is the simulation of the shear failure nearby the concentrated load, cohesive surfaces are used only within the three layers of bricks just under the steel plate. Both micro and homogenized models are re-run again with such a modification, leading to results even closer to the experimental ones. In terms of damage pattern (**Figure 21**), the results are quite close to the previous approaches, but with a shear failure more clearly defined.

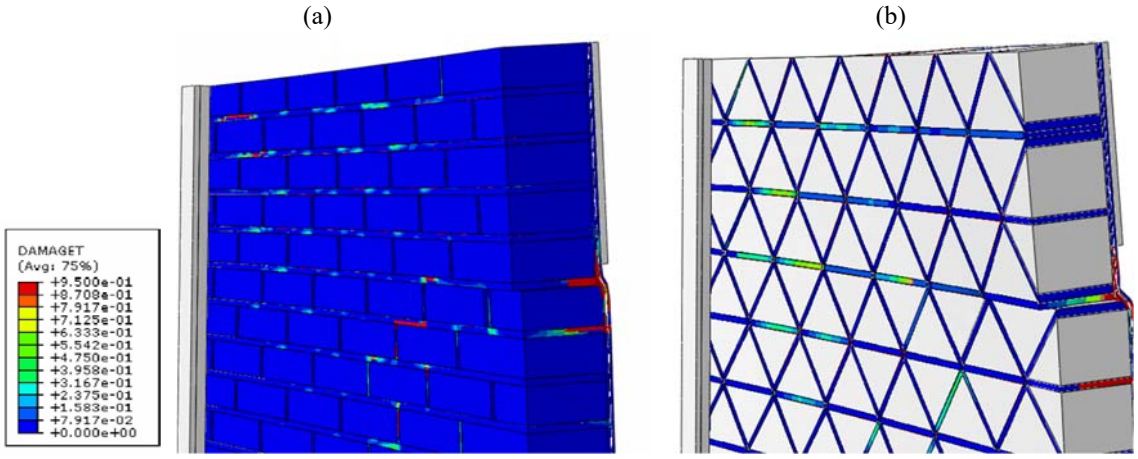

Figure 21. Damage pattern of micro-model reinforced panel (a) and homogenized reinforced panel (b) in presence of cohesive surfaces at the interfaces.

As far as the global behavior of the reinforced wall is concerned, the accuracy improves consistently for both cases. In **Figure 22,** the Load-Displacement curves labeled as “RE Micro Co” and “Re Homo Co” (i.e. the previous model with cohesive elements) are compared with tests and the previous numerical analyses. A very good match with experimental results is obtained when cohesive surfaces are introduced in the homogenized model. In fact, after a slight softening, the curve reproduces the plateau observed in the experimental tests, reaching an overall displacement of 55 mm.

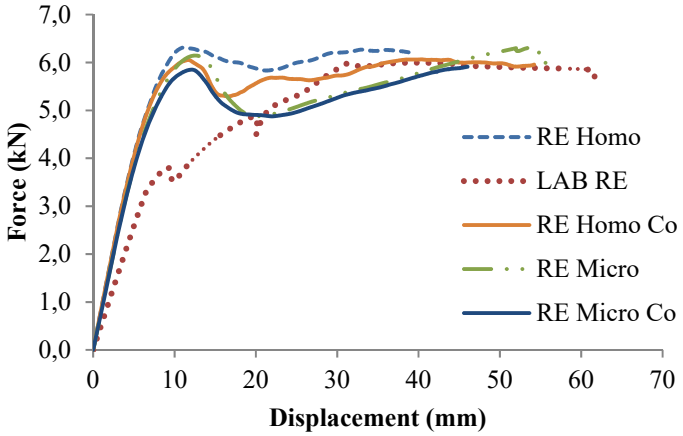

Figure 22. Comparison of the load-displacement curves of the reinforced panel for all the approaches.

7. REFERENCES

[1] C. Wang, V. Sarhosis, and N. Nikitas, "Strengthening/Retrofitting Techniques on Unreinforced Masonry Structure/Element Subjected to Seismic Loads: A Literature Review," *Open Constr. Build. Technol. J.*, vol. 12, no. 1, pp. 251–268, 2018.

[2] T. C. Triantafillou, "Strengthening of Masonry Structures Using Epoxy-Bonded FRP Laminates," *J. Compos. Constr.*, vol. 2, no. 2, pp. 96–104, 2002.

[3] E. Grande, G. Milani, and E. Sacco, "Modelling and analysis of FRP-strengthened masonry panels," *Eng. Struct.*, vol. 30, no. 7, pp. 1842–1860, 2008.

[4] M. R. Valluzzi *et al.*, "Round Robin Test for composite-to-brick shear bond characterization," *Mater. Struct. Constr.*, vol. 45, no. 12, pp. 1761–1791, 2012.

[5] G. de Felice *et al.*, "Experimental characterization of composite-to-brick masonry shear bond," *Mater. Struct. Constr.*, vol. 49, no. 7, pp. 2581–2596, 2016.

[6] A. Bellini and C. Mazzotti, "A review on the bond behavior of FRP composites applied on masonry substrates," *RILEM Tech. Lett.*, vol. 2, p. 74, 2017.

[7] B. Ghiassi, G. Marcari, D. V. Oliveira, and P. B. Lourenço, "Numerical analysis of bond behavior

between masonry bricks and composite materials," *Eng. Struct.*, vol. 43, pp. 210–220, 2012.

[8] B. Ghiassi, J. Xavier, D. V. Oliveira, and P. B. Lourenço, "Application of digital image correlation in investigating the bond between FRP and masonry," *Compos. Struct.*, vol. 106, pp. 340–349, 2013.

[9] T. Rotunno, M. Fagone, E. Bertolesi, E. Grande, and G. Milani, "Single lap shear tests of masonry curved pillars externally strengthened by CFRP strips," *Compos. Struct.*, vol. 200, no. April, pp. 434–448, 2018.

[10] A. Formisano, A. Iaquinandi, and F. M. Mazzolani, "Seismic retrofitting by FRP of a school building damaged by Emilia-Romagna earthquake," *Key Eng. Mater.*, vol. 624, pp. 106–113, 2015.

[11] T. C. Triantafillou, "A new generation of composite materials as alternative to fiber reinforced polymers for strengthening and seismic retrofitting of structures," in *Composite Materials. A vision for the future*, 2011.

[12] L. A. S. Kouris and T. C. Triantafillou, "State-of-the-art on strengthening of masonry structures with textile reinforced mortar (TRM)," *Constr. Build. Mater.*, vol. 188, pp. 1221–1233, 2018.

[13] A. D'Ambrisi, L. Feo, and F. Focacci, "Experimental and analytical investigation on bond between Carbon-FRCM materials and masonry," *Compos. Part B Eng.*, vol. 46, pp. 15–20, 2013.

[14] A. Bilotta, F. Ceroni, G. P. Lignola, and A. Prota, "Use of DIC technique for investigating the behaviour of FRCM materials for strengthening masonry elements," *Compos. Part B Eng.*, vol. 129, pp. 251–270, 2017.

[15] F. G. Carozzi *et al.*, "Experimental investigation of tensile and bond properties of Carbon-FRCM composites for strengthening masonry elements," *Compos. Part B Eng.*, vol. 128, pp. 100–119, 2017.

[16] B. Ghiassi *et al.*, "Round Robin Test on tensile and bond behaviour of Steel Reinforced Grout systems," *Compos. Part B Eng.*, vol. 127, pp. 100–120, 2017.

[17] R. Cardoso, M. Lopes, and R. Bento, "Seismic evaluation of old masonry buildings. Part I: Method description and application to a case-study," *Eng. Struct.*, vol. 27, no. 14, pp. 2024–2035, 2005.

[18] M. Leone *et al.*, "Glass fabric reinforced cementitious matrix: Tensile properties and bond performance on masonry substrate," *Compos. Part B Eng.*, vol. 127, pp. 196–214, 2017.

[19] L. Zuccarino *et al.*, "Performance assessment of basalt FRCM for retrofit applications on masonry,"

Compos. Part B Eng., vol. 128, pp. 1–18, 2017.

[20] N. Ismail and J. M. Ingham, "In-plane and out-of-plane testing of unreinforced masonry walls strengthened using polymer textile reinforced mortar," *Eng. Struct.*, vol. 118, pp. 167–177, 2016.

[21] L. Koutas, T. C. Triantafillou, and S. N. Bousias, "Analytical Modeling of Masonry-Infilled RC Frames Retrofitted with Textile-Reinforced Mortar," *J. Compos. Constr.*, vol. 19, no. 5, p. 04014082, 2014.

[22] A. Prota, G. Marcari, G. Fabbrocino, G. Manfredi, and C. Aldea, "Experimental In-Plane Behavior of Tuff Masonry Strengthened with Cementitious Matrix–Grid Composites," *J. Compos. Constr.*, vol. 10, no. 3, pp. 223–233, 2006.

[23] V. Alecci, M. De Stefano, F. Focacci, R. Luciano, L. Rovero, and G. Stipo, "Strengthening Masonry Arches with Lime-Based Mortar Composite," *Buildings*, vol. 7, no. 4, p. 49, 2017.

[24] M. De Stefano, V. Alecci, F. Focacci, G. Stipo, and L. Rovero, "Extrados strengthening of brick masonry arches with PBO–FRCM composites: Experimental and analytical investigations," *Compos. Struct.*, vol. 149, pp. 184–196, 2016.

[25] V. Alecci *et al.*, "Experimental investigation on masonry arches strengthened with PBO-FRCM composite," *Compos. Part B Eng.*, vol. 100, pp. 228–239, 2016.

[26] F. G. Carozzi, C. Poggi, E. Bertolesi, and G. Milani, "Ancient masonry arches and vaults strengthened with TRM, SRG and FRP composites: Experimental evaluation," *Compos. Struct.*, vol. 187, no. December 2017, pp. 466–480, 2018.

[27] L. Garmendia, P. Larrinaga, R. San-Mateos, and J. T. San-José, "Strengthening masonry vaults with organic and inorganic composites: An experimental approach," *Mater. Des.*, vol. 85, pp. 102–114, 2015.

[28] P. Foraboschi, "Resisting system and failure modes of masonry domes," *Eng. Fail. Anal.*, vol. 44, no. May, pp. 315–337, 2014.

[29] A. Cascardi, M. A. Aiello, and T. Triantafillou, "Analysis-oriented model for concrete and masonry confined with fiber reinforced mortar," *Mater. Struct. Constr.*, vol. 50, no. 4, 2017.

[30] P. E. Mezrea, I. A. Yilmaz, M. Ispir, E. Binbir, I. E. Bal, and A. Ilki, "External Jacketing of

Unreinforced Historical Masonry Piers with Open-Grid Basalt-Reinforced Mortar," *J. Compos. Constr.*, vol. 21, no. 3, p. 04016110, 2016.

[31] A. Formisano and A. Marzo, "Simplified and refined methods for seismic vulnerability assessment and retrofitting of an Italian cultural heritage masonry building," *Comput. Struct.*, vol. 180, pp. 13–26, 2017.

[32] M. Mosoarca, I. Apostol, A. Keller, and A. Formisano, "Consolidation methods of Romanian historical building with composite materials," *Key Eng. Mater.*, vol. 747 KEM, no. July, pp. 406–413, 2017.

[33] A. Formisano, G. Vaiano, and F. Fabbrocino, "Seismic and energetic interventions on a typical south Italy residential building: Cost analysis and tax detraction," *Front. Built Environ.*, vol. 5, no. February, pp. 1–15, 2019.

[34] A. M. D'Altri *et al.*, *Modeling Strategies for the Computational Analysis of Unreinforced Masonry Structures: Review and Classification*. Springer Netherlands, 2019.

[35] A. M. D'Altri, S. de Miranda, G. Castellazzi, and V. Sarhosis, "A 3D detailed micro-model for the in-plane and out-of-plane numerical analysis of masonry panels," *Comput. Struct.*, vol. 206, pp. 18–30, 2018.

[36] V. Sarhosis and J. V. Lemos, "A detailed micro-modelling approach for the structural analysis of masonry assemblages," *Comput. Struct.*, vol. 206, pp. 66–81, 2018.

[37] P. B. Lourenço, R. De Borst, and J. G. Rots, "A plane stress softening plasticity model for orthotropic materials," *Int. J. Numer. Methods Eng.*, vol. 40, no. 21, pp. 4033–4057, 1997.

[38] R. Luciano and E. Sacco, "Homogenization technique and damage model for old masonry material," *Int. J. Solids Struct.*, vol. 34, no. 24, pp. 3191–3208, 1997.

[39] G. Milani, "Simple homogenization model for the non-linear analysis of in-plane loaded masonry walls," *Comput. Struct.*, vol. 89, no. 17–18, pp. 1586–1601, 2011.

[40] G. Milani and E. Bertolesi, "Quasi-analytical homogenization approach for the non-linear analysis of in-plane loaded masonry panels," *Constr. Build. Mater.*, vol. 146, pp. 723–743, 2017.

[41] S. Casolo and G. Milani, "A simplified homogenization-discrete element model for the non-linear

static analysis of masonry walls out-of-plane loaded," *Eng. Struct.*, vol. 32, no. 8, pp. 2352–2366, 2010.

[42] E. Bertolesi, G. Milani, and C. Poggi, "Simple holonomic homogenization model for the non-linear static analysis of in-plane loaded masonry walls strengthened with FRCM composites," *Compos. Struct.*, vol. 158, pp. 291–307, 2016.

[43] E. Bertolesi, G. Milani, and S. Casolo, "Homogenization towards a mechanistic Rigid Body and Spring Model (HRBSM) for the non-linear dynamic analysis of 3D masonry structures," *Meccanica*, vol. 53, no. 7, pp. 1819–1855, 2018.

[44] E. Bertolesi, G. Milani, and P. B. Lourenço, "Implementation and validation of a total displacement non-linear homogenization approach for in-plane loaded masonry," *Comput. Struct.*, vol. 176, pp. 13–33, 2016.

[45] C. D'Ambra, G. P. Lignola, A. Prota, E. Sacco, and F. Fabbrocino, "Experimental performance of FRCM retrofit on out-of-plane behaviour of clay brick walls," *Compos. Part B Eng.*, vol. 148, no. January, pp. 198–206, 2018.

[46] SIMULIA, *ABAQUS. Finite Element Analys, Release 6.13 Theory Manual*. Maastricht, 2006.

[47] E. Bertolesi, F. G. Carozzi, G. Milani, and C. Poggi, "Numerical modeling of Fabric Reinforce Cementitious Matrix composites (FRCM) in tension," *Constr. Build. Mater.*, vol. 70, pp. 531–548, 2014.

[48] L. C. Silva, P. B. Lourenço, and G. Milani, "Nonlinear Discrete Homogenized Model for Out-of-Plane Loaded Masonry Walls," *J. Struct. Eng.*, vol. 143, no. 9, p. 04017099, 2017.

[49] K. F. Abdulla, L. S. Cunningham, and M. Gillie, "Simulating masonry wall behaviour using a simplified micro-model approach," *Eng. Struct.*, vol. 151, pp. 349–365, 2017.